

U-shaped Vision Mamba for Single Image Dehazing

Zhuoran Zheng¹ and Chen Wu²

¹ Nanjing University of Science and Technology

² University of Science and Technology of China
zhengzr@njust.edu.cn

Abstract. Currently, Transformer is the most popular architecture for image dehazing, but due to its large computational complexity, its ability to handle long-range dependency is limited on resource-constrained devices. To tackle this challenge, we introduce the U-shaped Vision Mamba (UVM-Net), an efficient single-image dehazing network. Inspired by the State Space Sequence Models (SSMs), a new deep sequence model known for its power to handle long sequences, we design a Bi-SSM block that integrates the local feature extraction ability of the convolutional layer with the ability of the SSM to capture long-range dependencies. Extensive experimental results demonstrate the effectiveness of our method. Our method provides a more highly efficient idea of long-range dependency modeling for image dehazing as well as other image restoration tasks. The URL of the code is <https://github.com/zxr-idam>.

Keywords: Transformer · Image dehazing · UVM-Net · SSMs.

1 Introduction

Haze is a common atmospheric phenomenon that interferes with people’s daily life as well as their judgment of goals, and heavy haze can even impact traffic safety. For computer vision, haze reduces the quality of images in most cases. It affects the model reliability in advanced vision tasks, further misleading machine systems, such as autonomous driving. Therefore, to perform efficient image dehazing through algorithms is a necessary work.

Single image dehazing aims to estimate the sharp image given a hazy input, which is a highly ill-posed problem. Conventional approaches are physically inspired and apply various sharp image priors [20,12,52,2] to regularize the solution space. However, these methods depend on manual priors, and real-world haze is more complex than the preset priors. Recently, deep learning approaches have shown promising performance [4,38,50,26,39,30,5,11,9,10,36,45,42,40], especially image dehazing methods based on Transformer’s architecture [41].

Although these approaches achieve state-of-the-art results on a single image dehazing task, their models usually have a large size of parameters and are computationally expensive. Note that self-attention mechanisms are quadratically proportional to the size of the input image, thus making them resource-

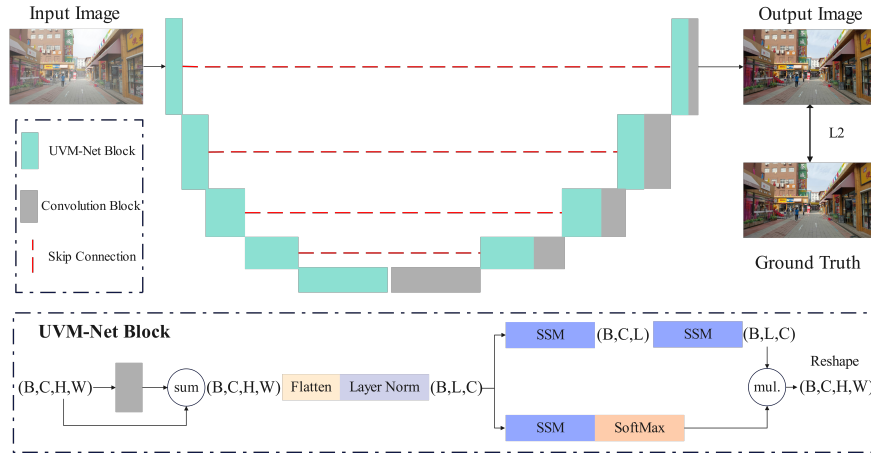


Fig. 1. Overview of the UVM-Net architecture. UVM-Net employs the encoder-decoder framework with UVM-Net blocks in the encoder and convolution blocks in the decoder, together with skip connections. In UVM-Net block, our feature maps are first applied to a convolution operation, then the unfolded pixels are modeled over SSM, and the size of the final feature is reshaped to the size of the input information.

intensive, especially for hazy images with high resolution that are usually available. Therefore, how to have efficient modeling of long-range dependencies of images remains an unresolved issue. Recently, State Space Sequence Models (SSMs) [16,19], especially Structured State Space Sequence Models (S4) [18], have emerged as efficient building blocks (or layers) for constructing deep networks, and have gained promising performances in the analysis of continuous long sequence data [15,18]. Recently, mamba [17] demonstrated excellent modeling capabilities for long-range dependencies, and it performed well for image [34] and video [23] classification, and medical image segmentation [31,43].

Inspired by U-Mamba [31] and Mamba-UNet [43], we present a U-shaped Vision Mamba (UVM-Net), which forms a deep network based on the U-Net structure with both local capture capability and efficient long-range modeling. Unlike U-Mamba and Mamba-UNet, we propose the Bi-SSM module, where we scroll the feature maps over the channel domain to fully utilize the long-range modeling capability of SSM. U-Mamba and Mamba-UNet do not build a long-range dependency on another dimension of the feature map (the non-channel domain). Extensive experimental results demonstrate that our method performs well on the task of image dehazing. UVM-NET paves the way for future advances in network design that can show additional capabilities in other image restoration tasks.

Table 1. Quantitative comparison of various dehazing methods trained on the RE-SIDE datasets.

Methods	ITS		OTS		RESIDE-6K		RS-Haze		Overhead	
	SOTS-indoor		SOTS-outdoor		SOTS-mix		RS-Haze-mix		#Param	MACs
	PSNR	SSIM	PSNR	SSIM	PSNR	SSIM	PSNR	SSIM		
(TPAMI'10) DCP [20]	16.62	0.818	19.13	0.815	17.88	0.816	17.86	0.734	-	-
(TIP'16) DehazeNet [4]	19.82	0.821	24.75	0.927	21.02	0.870	23.16	0.816	0.009M	0.581G
(ECCV'16) MSCNN [38]	19.84	0.833	22.06	0.908	20.31	0.863	22.80	0.823	0.008M	0.525G
(ICCV'17) AOD-Net [26]	20.51	0.816	24.14	0.920	20.27	0.855	24.90	0.830	0.002M	0.115G
(CVPR'18) GFN [39]	22.30	0.880	21.55	0.844	23.52	0.905	29.24	0.910	0.499M	14.94G
(WACV'19) GCANet [5]	30.23	0.980	-	-	25.09	0.923	34.41	0.949	0.702M	18.41G
(ICCV'19) GridDehazeNet [30]	32.16	0.984	30.86	0.982	25.86	0.944	36.40	0.960	0.956M	21.49G
(CVPR'20) MSBDN [10]	33.67	0.985	33.48	0.982	28.56	0.966	38.57	0.965	31.35M	41.54G
(ECCV'20) PFDN [11]	32.68	0.976	-	-	28.15	0.962	36.04	0.955	11.27M	50.46G
(AAAI'20) FFA-Net [36]	36.39	0.989	33.57	0.984	29.96	0.973	39.39	0.969	4.456M	287.8G
(CVPR'21) AECR-Net [45]	37.17	0.990	-	-	28.52	0.964	35.69	0.959	2.611M	52.20G
DehazeFormer-T [41]	35.15	0.989	33.71	0.982	30.36	0.973	39.11	0.968	0.686M	6.658G
DehazeFormer-S [41]	36.82	0.992	34.36	0.983	30.62	0.976	39.57	0.970	1.283M	13.13G
DehazeFormer-B [41]	37.84	0.994	34.95	0.984	31.45	0.980	39.87	0.971	2.514M	25.79G
DehazeFormer-M [41]	38.46	0.994	34.29	0.983	30.89	0.977	39.71	0.971	4.634M	48.64G
DehazeFormer-L [41]	40.05	0.996	-	-	-	-	-	-	25.44M	279.7G
Ours	40.17	0.996	34.92	0.984	31.92	0.982	39.88	0.972	19.25M	173.55G

2 Method

UVM-Net follows the encoder-decoder network architecture that captures both local features and long-range information efficiently. Fig. 1 shows an overview of the UVM-Net block and the whole network architecture. Next, we first introduce the Mamba block followed by illustrating the details of UVM-Net.

2.1 UVM-Net

Mamba has demonstrated impressive results on a variety of discrete data, but it remains underexplored in the field of image dehazing. Here, we take advantage of Mamba’s linear scaling to enhance the long-range dependency modeling of traditional U-Net.

As shown in Fig. 1, each building block contains two successive convolution blocks [21] followed by a UVM-net block. The convolution block contains the standard convolutional layer ($\times 3$) with Leaky ReLU [32]. Image features with a shape of (B, C, H, W) are then flattened and transposed to (B, L, C) where $L = H \times W \times D$. After passing the Layer Normalization [1], the features enter the Mamba block [17] that contains two parallel branches. In the first branch, the features are expanded to (B, L, C) by a SSM layer, next, the roll transforms into an (B, C, L) before entering an SSM. In the second branch, the features are also expanded to (B, L, C) by a SSM layer, next, the feature map goes through softmax to form an attention map. Then, the features from the two branches are merged with the Hadamard product. Finally, the features are projected back to the original shape (B, L, C) and then reshaped and transposed to (B, C, H, W) . The entire model down-sampling and up-sampling of the feature map is consistent with standard U-Net, notably the bilinear interpolation used for up-sampling.

3 Experiments

The setup of the experiment follows exactly Dehazeformer’s [41] configuration in the paper, including the number of iterations, the learning rate, and the batch size. This is because it is currently the SOTA in the field of single-image dehazing and our structure is similar to it. For this paper, we used PyTorch 1.8 and the GPU was a 3090RTX shader with 48G RAM. We use the number of parameters (#Param) and multiply-accumulate operations (MACs) to measure the overhead. MACs are measured on 256×256 images.

3.1 Quantitative Comparison

We quantitatively compare the performance of UVM-Net and baselines, and the results are shown in TABLE 1. Here we bold the results where UVM-Net exceeds them. Overall, our proposed UVM-Net outperformed these baselines.

3.2 Qualitative Comparison

We compared with dehazeformer on the publicly available dataset and the real-world image with haze, where dehazeformer is over-enhanced on the publicly available dataset.

3.3 Ablation Study

We perform ablation studies on the RESIDE-Full’s indoor scene. We conducted two ablation experiments where 1) we removed the SSM to use 1D convolution instead, and 2) we removed the SSM to use scaled dot product instead. The experimental results show the effectiveness of our method.

Table 2. Ablation study on SSM module.

Setting	PSNR	SSIM	#Param	MACs
Ours	39.88	0.972	19.25M	173.55G
1D conv	35.11	0.950	10.66M	88.93G
SDP	38.25	0.968	23.88M	229.93G

4 Other task

Low light enhancement. We evaluate the performance of our method on two paired public datasets, including the LOL dataset [7] and the MIT-Adobe FiveK

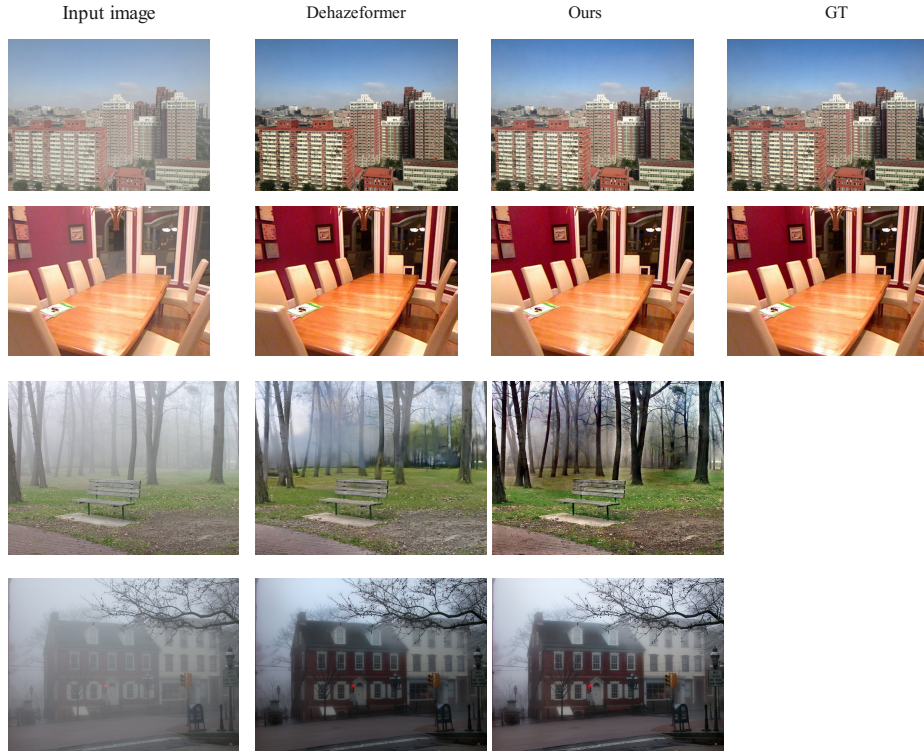


Fig. 2. Qualitative comparison of image dehazing methods on SOTS mix set, where the first rows are outdoor images, and the second row is indoor images. The third and fourth rows are real-world images. The first column is the hazy images and the last is the corresponding ground truth.

dataset [3] (see Table 3). We randomly select 450 pairs divided in the dataset for training and the other 50 pairs for testing. Each pair contains a low-light image and its corresponding well-exposed reference image. MIT-Adobe FiveK contains 5000 images recorded with a DSLR camera, and the tonal attributes of all images are manually adjusted by five photographic experts (A/B/C/D/E). Reference with [22], we use the retouched results of expert C as the ground truth. We manually divide the MIT-Adobe FiveK dataset into two parts at a ratio of 8:2, using the first 4000 images to train the model and randomly selecting 500 images from the remaining images for testing. We uniformly convert the raw images in the above dataset to PNG format for training and testing. The Implementation of the environment uses the PyTorch [35] open-source framework, trained and tested on Intel(R) Xeon(R) Gold 5218 CPU @ 2.30GHz, 128G RAM, and TITAN RTX3090 GPU with 24G RAM. We set the batch size to 12 and trained our model using the AdamW optimizer with $\beta_1 = 0.9$, $\beta_2 = 0.999$, and $\epsilon = 10^{-8}$.

Table 3. Compare quantization with the state-of-the-art image enhancement methods in LOL and MIT-Adobe FiveK (MIT5K).

		BIMEF	CRM	LIME	RetinexNet	MBLLEN	DSLR	DRBN	ZeroDCE++	KinD++	TFR	Ours
LOL	PSNR \uparrow	13.88	17.20	16.76	16.77	17.56	18.24	20.13	19.43	21.30	22.92	24.32
	SSIM \uparrow	0.577	0.644	0.564	0.567	0.736	0.787	0.802	0.768	0.822	0.837	0.859
	NIQE \downarrow	7.69	8.02	9.13	9.73	3.46	4.11	4.63	7.79	5.11	4.03	3.92
MIT5K	PSNR \uparrow	18.67	13.99	11.21	20.81	16.42	17.02	20.95	16.46	22.01	25.03	25.78
	SSIM \uparrow	0.693	0.674	0.667	0.687	0.851	0.750	0.794	0.766	0.832	8.521	0.925
	NIQE \downarrow	3.87	4.22	4.50	4.48	4.19	3.90	5.44	3.92	4.15	3.49	3.40

Table 4. Comparison of quantitative results on five benchmark datasets. Best and second best values are indicated with **bold** text and underlined text respectively.

Datasets Methods	Test100		Rain100H		Rain100L		Test1200		Test2800		Average	
	PSNR	SSIM	PSNR	SSIM	PSNR	SSIM	PSNR	SSIM	PSNR	SSIM	PSNR	SSIM
DerainNet [13]	22.77	0.810	14.92	0.592	27.03	0.884	24.31	0.861	23.38	0.835	22.48	0.796
SEMI [44]	22.35	0.788	16.56	0.486	25.03	0.842	24.43	0.782	26.05	0.822	22.88	0.744
DIDMDN [51]	22.56	0.818	17.35	0.524	25.23	0.741	28.13	0.867	29.95	0.901	24.58	0.770
UMRL [48]	24.41	0.829	26.01	0.832	29.18	0.923	29.97	0.905	30.55	0.910	28.02	0.880
RESCAN [28]	25.00	0.835	26.36	0.786	29.80	0.881	31.29	0.904	30.51	0.882	28.59	0.857
PReNet [37]	24.81	0.851	26.77	0.858	32.44	0.950	31.75	0.916	31.36	0.911	29.42	0.897
MSPFN [24]	27.50	0.876	28.66	0.860	32.40	0.933	32.82	0.930	32.39	0.916	30.75	0.903
MPRNet [49]	30.27	0.897	30.41	0.890	36.40	0.965	33.64	0.938	32.91	0.916	32.73	0.921
KiT [25]	30.26	0.904	30.47	0.897	36.65	0.969	33.85	0.941	32.81	0.918	32.81	0.929
DGUNet [33]	30.32	0.899	30.66	0.891	37.42	0.969	33.68	0.938	33.23	0.920	33.06	0.923
IDT [46]	29.69	0.905	29.95	0.898	37.01	0.971	33.38	0.937	31.38	0.908	32.28	0.924
HINet [6]	30.26	0.905	30.63	0.893	37.20	0.969	33.87	0.940	33.01	0.918	33.00	0.925
DCT [29]	30.91	0.912	<u>30.74</u>	0.892	38.19	<u>0.974</u>	<u>33.89</u>	<u>0.941</u>	<u>33.57</u>	<u>0.926</u>	<u>33.46</u>	<u>0.929</u>
SFNet [8]	<u>31.47</u>	<u>0.919</u>	31.90	<u>0.908</u>	<u>38.21</u>	<u>0.974</u>	33.69	0.937	32.55	0.911	<u>33.56</u>	<u>0.929</u>
Ours	32.11	0.915	30.66	0.909	39.66	0.985	34.92	0.942	33.89	0.952	33.98	0.940

The learning rate is initialized to 0.0001, and 200 epochs are enforced, decaying by a factor of 0.5 in every 50 epochs.

Deraining. we conduct extensive experiments on the Rain13K training dataset which contains 13700 clean/rain image pairs. For the testing, five synthetic benchmarks (Test100 [27], Rain100H [47], Rain100L [47], Test2800 [14], and Test1200 [14]) are considered for evaluation. For each image used, we use BLIP to generate corresponding text descriptions. We calculate the PSNR and SSIM along the Y channel in the YCbCr color space as quantitative comparisons. We compare our method with 14 image deraining approaches, including DerainNet [13], SEMI [44], DIDMDN [51], UMRL [48], RESCAN [28], PReNet [37], MSPFN [24], MPRNet [49], KiT [25], DGUNet [33], IDT [46], HINet [6], DCT [29] and SFNet [8]. In Tab. 4, we report the quantitative comparison results among different methods. We conduct experiments in PyTorch on NVIDIA GeForce RTX 3090 GPUs. The network is trained for a total of 300k iterations with a batch size of 8. The initial learning rate is 2×10^{-4} , and the Adam optimizer is used to decay with the cosine annealing schedule. During training, we utilize cropped patches of size 128×128 as input, and to augment the training data, random horizontal and vertical flips are applied to the input images.

5 Discussion

Our model is a potentially large visual model (3.9G weight file). Limited by the consumer GPU's RAM, the fixed weight of 64 can be increased to 256 if the number of GPUs is sufficient.

6 Conclusion

In this paper, we present a new architecture, UVM-Net, for single image dehazing, which integrates the advantages of local mode recognition of CNN and global context understanding of SSM. The results show that UVM-Net has the promise to be the backbone of promising image restoration networks for the next generation.

References

1. Ba, J.L., Kiros, J.R., Hinton, G.E.: Layer normalization. arXiv preprint arXiv:1607.06450 (2016) [3](#)
2. Berman, D., Avidan, S., et al.: Non-local image dehazing. In: CVPR. pp. 1674–1682 (2016) [1](#)
3. Bychkovsky, V., Paris, S., Chan, E., Durand, F.: Learning photographic global tonal adjustment with a database of input/output image pairs. In: CVPR 2011. pp. 97–104. IEEE (2011) [5](#)
4. Cai, B., Xu, X., Jia, K., Qing, C., Tao, D.: Dehazenet: An end-to-end system for single image haze removal. IEEE TIP **25**(11), 5187–5198 (2016) [1, 3](#)
5. Chen, D., He, M., Fan, Q., Liao, J., Zhang, L., Hou, D., Yuan, L., Hua, G.: Gated context aggregation network for image dehazing and deraining. In: WACV. pp. 1375–1383 (2019) [1, 3](#)
6. Chen, L., Lu, X., Zhang, J., Chu, X., Chen, C.: Hinet: Half instance normalization network for image restoration. In: CVPR. pp. 182–192 (2021) [6](#)
7. Chen Wei, Wenjing Wang, W.Y.J.L.: Deep retinex decomposition for low-light enhancement. In: British Machine Vision Conference (2018) [4](#)
8. Cui, Y., Tao, Y., Bing, Z., Ren, W., Gao, X., Cao, X., Huang, K., Knoll, A.: Selective frequency network for image restoration. In: ICLR (2022) [6](#)
9. Deng, Q., Huang, Z., Tsai, C.C., Lin, C.W.: Hardgan: A haze-aware representation distillation gan for single image dehazing. In: ECCV. pp. 722–738. Springer (2020) [1](#)
10. Dong, H., Pan, J., Xiang, L., Hu, Z., Zhang, X., Wang, F., Yang, M.H.: Multi-scale boosted dehazing network with dense feature fusion. In: CVPR. pp. 2157–2167 (2020) [1, 3](#)
11. Dong, J., Pan, J.: Physics-based feature dehazing networks. In: ECCV. pp. 188–204. Springer (2020) [1, 3](#)
12. Fattal, R.: Dehazing using color-lines. ACM TOG **34**(1), 1–14 (2014) [1](#)
13. Fu, X., Huang, J., Ding, X., Liao, Y., Paisley, J.: Clearing the skies: A deep network architecture for single-image rain removal. TIP **26**(6), 2944–2956 (2017) [6](#)
14. Fu, X., Huang, J., Zeng, D., Huang, Y., Ding, X., Paisley, J.: Removing rain from single images via a deep detail network. In: CVPR. pp. 3855–3863 (2017) [6](#)

15. Goel, K., Gu, A., Donahue, C., Ré, C.: It's raw! audio generation with state-space models. In: International Conference on Machine Learning. pp. 7616–7633 (2022) [2](#)
16. Gu, A.: Modeling Sequences with Structured State Spaces. Phd thesis, Stanford University (2023), proQuest Document ID: 2880853867 [2](#)
17. Gu, A., Dao, T.: Mamba: Linear-time sequence modeling with selective state spaces. arXiv preprint arXiv:2312.00752 (2023) [2](#), [3](#)
18. Gu, A., Goel, K., Re, C.: Efficiently modeling long sequences with structured state spaces. In: International Conference on Learning Representations (2021) [2](#)
19. Gu, A., Johnson, I., Goel, K., Saab, K., Dao, T., Rudra, A., Ré, C.: Combining recurrent, convolutional, and continuous-time models with linear state space layers. *Advances in Neural Information Processing Systems* **34**, 572–585 (2021) [2](#)
20. He, K., Sun, J., Tang, X.: Single image haze removal using dark channel prior. *IEEE TPAMI* **33**(12), 2341–2353 (2010) [1](#), [3](#)
21. He, K., Zhang, X., Ren, S., Sun, J.: Deep residual learning for image recognition. In: Proceedings of the IEEE Conference on Computer Vision and Pattern Recognition. pp. 770–778 (2016) [3](#)
22. Hu, Y., He, H., Xu, C., Wang, B., Lin, S.: Exposure: A white-box photo post-processing framework. *ACM Trans. Graph.* **37**(2), 1–17 (2018) [5](#)
23. Islam, M.M., Bertasius, G.: Long movie clip classification with state-space video models. In: European Conference on Computer Vision. pp. 87–104 (2022) [2](#)
24. Jiang, K., Wang, Z., Yi, P., Chen, C., Huang, B., Luo, Y., Ma, J., Jiang, J.: Multi-scale progressive fusion network for single image deraining. In: CVPR. pp. 8346–8355 (2020) [6](#)
25. Lee, H., Choi, H., Sohn, K., Min, D.: Knn local attention for image restoration. In: CVPR. pp. 2139–2149 (2022) [6](#)
26. Li, B., Peng, X., Wang, Z., Xu, J., Feng, D.: Aod-net: All-in-one dehazing network. In: ICCV. pp. 4770–4778 (2017) [1](#), [3](#)
27. Li, S., Araujo, I.B., Ren, W., Wang, Z., Tokuda, E.K., Junior, R.H., Cesar-Junior, R., Zhang, J., Guo, X., Cao, X.: Single image deraining: A comprehensive benchmark analysis. In: CVPR. pp. 3838–3847 (2019) [6](#)
28. Li, X., Wu, J., Lin, Z., Liu, H., Zha, H.: Recurrent squeeze-and-excitation context aggregation net for single image deraining. In: ECCV. pp. 254–269 (2018) [6](#)
29. Li, Y., Lu, J., Chen, H., Wu, X., Chen, X.: Dilated convolutional transformer for high-quality image deraining. In: CVPR. pp. 4198–4206 (2023) [6](#)
30. Liu, X., Ma, Y., Shi, Z., Chen, J.: Griddehazenet: Attention-based multi-scale network for image dehazing. In: ICCV. pp. 7314–7323 (2019) [1](#), [3](#)
31. Ma, J., Li, F., Wang, B.: U-mamba: Enhancing long-range dependency for biomedical image segmentation. arXiv preprint arXiv:2401.04722 (2024) [2](#)
32. Maas, A.L., Hannun, A.Y., Ng, A.Y., et al.: Rectifier nonlinearities improve neural network acoustic models. In: International Conference on Machine Learning. vol. 28 (2013) [3](#)
33. Mou, C., Wang, Q., Zhang, J.: Deep generalized unfolding networks for image restoration. In: CVPR. pp. 17399–17410 (2022) [6](#)
34. Nguyen, E., Goel, K., Gu, A., Downs, G., Shah, P., Dao, T., Baccus, S., Ré, C.: S4nd: Modeling images and videos as multidimensional signals with state spaces. In: *Advances in Neural Information Processing Systems*. vol. 35, pp. 2846–2861 (2022) [2](#)
35. Paszke, A., Gross, S., Massa, F., Lerer, A., Bradbury, J., Chanan, G., Killeen, T., Lin, Z., Gimelshein, N., Antiga, L., et al.: Pytorch: An imperative style, high-performance deep learning library. arXiv preprint arXiv:1912.01703 (2019) [5](#)

36. Qin, X., Wang, Z., Bai, Y., Xie, X., Jia, H.: Ffa-net: Feature fusion attention network for single image dehazing. In: AAAI. pp. 11908–11915 (2020) [1](#), [3](#)
37. Ren, D., Zuo, W., Hu, Q., Zhu, P., Meng, D.: Progressive image deraining networks: A better and simpler baseline. In: CVPR. pp. 3937–3946 (2019) [6](#)
38. Ren, W., Liu, S., Zhang, H., Pan, J., Cao, X., Yang, M.H.: Single image dehazing via multi-scale convolutional neural networks. In: ECCV. pp. 154–169 (2016) [1](#), [3](#)
39. Ren, W., Ma, L., Zhang, J., Pan, J., Cao, X., Liu, W., Yang, M.H.: Gated fusion network for single image dehazing. In: CVPR. pp. 3253–3261 (2018) [1](#), [3](#)
40. Shao, Y., Li, L., Ren, W., Gao, C., Sang, N.: Domain adaptation for image dehazing. In: CPVR. pp. 2808–2817 (2020) [1](#)
41. Song, Y., He, Z., Qian, H., Du, X.: Vision transformers for single image dehazing. *IEEE Transactions on Image Processing* **32**, 1927–1941 (2023) [1](#), [3](#), [4](#)
42. Wang, C., Shen, H.Z., Fan, F., Shao, M.W., Yang, C.S., Luo, J.C., Deng, L.J.: Eaa-net: A novel edge assisted attention network for single image dehazing. *KBS* **228**, 107279 (2021) [1](#)
43. Wang, Z., Zheng, J.Q., Zhang, Y., Cui, G., Li, L.: Mamba-unet: Unet-like pure visual mamba for medical image segmentation. arXiv preprint arXiv:2402.05079 (2024) [2](#)
44. Wei, W., Meng, D., Zhao, Q., Xu, Z., Wu, Y.: Semi-supervised transfer learning for image rain removal. In: CVPR. pp. 3877–3886 (2019) [6](#)
45. Wu, H., Qu, Y., Lin, S., Zhou, J., Qiao, R., Zhang, Z., Xie, Y., Ma, L.: Contrastive learning for compact single image dehazing. In: CVPR. pp. 10551–10560 (2021) [1](#), [3](#)
46. Xiao, J., Fu, X., Liu, A., Wu, F., Zha, Z.J.: Image de-raining transformer. *TPAMI* (2022) [6](#)
47. Yang, W., Tan, R.T., Feng, J., Liu, J., Guo, Z., Yan, S.: Deep joint rain detection and removal from a single image. In: CVPR. pp. 1357–1366 (2017) [6](#)
48. Yasarla, R., Patel, V.M.: Uncertainty guided multi-scale residual learning-using a cycle spinning cnn for single image de-raining. In: CVPR. pp. 8405–8414 (2019) [6](#)
49. Zamir, S.W., Arora, A., Khan, S., Hayat, M., Khan, F.S., Yang, M.H., Shao, L.: Multi-stage progressive image restoration. In: CVPR. pp. 14821–14831 (2021) [6](#)
50. Zhang, H., Patel, V.M.: Densely connected pyramid dehazing network. In: CVPR. pp. 3194–3203 (2018) [1](#)
51. Zhang, H., Patel, V.M.: Density-aware single image de-raining using a multi-stream dense network. In: CVPR. pp. 695–704 (2018) [6](#)
52. Zhu, Q., Mai, J., Shao, L.: A fast single image haze removal algorithm using color attenuation prior. *IEEE TIP* **24**(11), 3522–3533 (2015) [1](#)